Journal of ELECTRONIC MATERIALS, Vol. 43, No. 12, 2014
DOI: 10.1007/s11664-014-3383-z

Polarization Effects of GaN and AlGaN: Polarization Bound Charge, Band Bending, and Electronic Surface States

BRIANNA S. ELLER,[1] JIALING YANG,[1] and ROBERT J. NEMANICH[1,2]

1.—Department of Physics, Arizona State University, Tempe, AZ 85287-1504, USA. 2.—e-mail: robert.nemanich@asu.edu

GaN-based devices are currently limited by reliability issues such as gate leakage and current collapse, where the mechanisms responsible for degradation are closely related to the electronic surface state configuration. Therefore, understanding the electronic surface state configuration of GaN-based materials will help improve device performance. Since GaN has an inherent polarization, these materials are also subject to a bound polarization charge, which influences the electronic state configuration. In this study, the surface band bending of N-face GaN, Ga-face GaN, and Ga-face AlGaN was measured with x-ray photoemission spectroscopy after various cleaning steps to investigate the effects of the polarization. Despite the different surface bound charge on these materials, similar band bending was observed regardless of the magnitude or direction of the charge. Specifically, the band bending varied from −0.1 eV to 0.9 eV on these samples, which supported the models of a Fermi level pinning state at ∼0.4 eV to 0.8 eV below the conduction band. Based on available literature, we suggest this pinning state is indirectly evident of a nitrogen vacancy or gallium-dangling bond.

Key words: GaN, AlGaN, polarization, surface states, band bending

INTRODUCTION

Mitigating multi-lateral ecological and environmental concerns will define next-generation technology. In particular, improvement in power electronic technologies ensures progress towards this goal. GaN-based semiconductors thus remain promising candidates, where GaN has several advantages over competing semiconductors in power applications—e.g., Si, SiC, and GaAs—due to superlative material properties.[1] Specifically, GaN is characterized by high power per unit width, which allows for smaller devices, easier manufacturing, and higher impedance. This characteristic also facilitates system matching that may be difficult with other materials such as GaAs. Moreover, the high breakdown field of GaN supports higher operating voltages, reduced voltage conversion, decreased power requirements, and simpler cooling. Consequently, many GaN-based devices have demonstrated superior performance.[2] However, despite the success of GaN-based devices, there are three issues that require resolution before GaN technology can replace existing Si technology: (1) the development of high-quality growth methods of single-crystal epitaxial GaN, (2) the selective formation of regions, and (3) the minimization of electronic states at the gate dielectric and GaN or AlGaN interface.[3] In this article, we address the last one. More specifically, this work investigates the effects of the polarization bound charge associated with III–V nitrides on surface states in an attempt to reveal relevant pinning states. In particular, this work focuses on oxygen-terminated surfaces, which are more representative of the conditions at the device interface. Results of these oxygen-terminated surfaces show band bending is independent of the magnitude or direction of the polarization; these similarities indicate a likely pinning surface state located ∼0.4 eV to 0.8 eV below the conduction band that can accommodate both positive and negative

(Received June 9, 2014; accepted August 16, 2014; published online September 6, 2014)

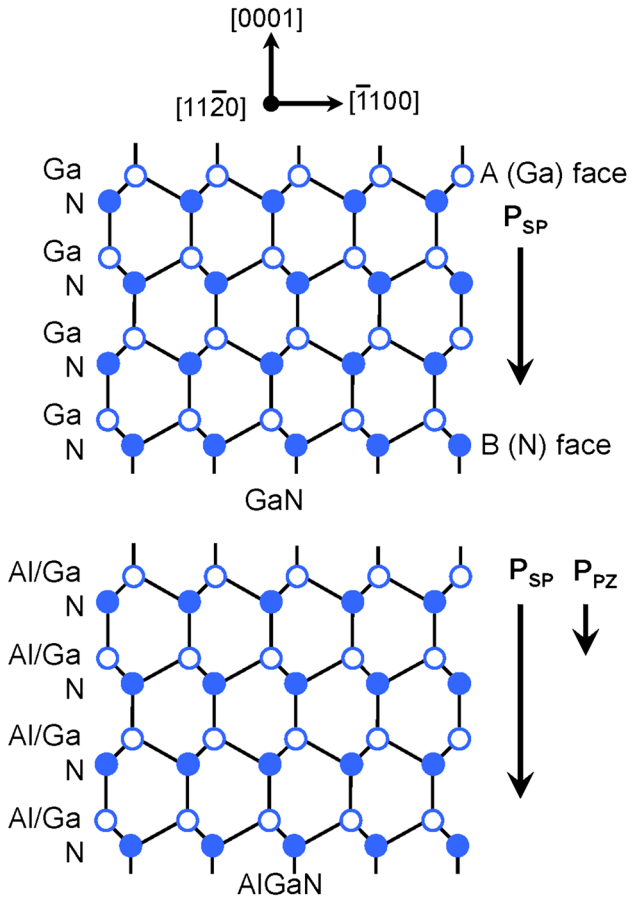

Fig. 1. (Color online) Crystal structure, spontaneous polarization fields (P_{SP}), and piezoelectric polarization fields (P_{PE}) for GaN (top) and $Al_xGa_{(1-x)}N$ (bottom). Reprinted from Yu et al.[18] ©1999, American Vacuum Society.

charge. Based on available literature, we suggest the relevant pinning state is likely related to the nitrogen vacancy or gallium-dangling bond.

Unlike Si, GaN and other wurtzite, III–V nitrides are characterized by a macroscopic polarization, $\bar{P}$. This polarization arises from the material properties of the nitrides, where $\bar{P}$ is the sum of the spontaneous polarization inherent to the equilibrium lattice, $\bar{P}_{\mathrm{SP}}$, and the piezoelectric polarization created by strain, $\bar{P}_{\mathrm{PE}}$. (See Fig. 1.) Using ab initio calculations and material constants, the polarization along the c-axis as induced by the piezoelectric effect is

$$\bar{P}_{\mathrm{PE}} = 2\frac{a-a_o}{a_o}\left(e_{31} - \frac{C_{13}}{C_{33}}e_{33}\right)\hat{c}, \tag{1}$$

where C_{13} and C_{33} are elastic constants, e_{31} and e_{33} are piezoelectric coefficients, and a_o and a are lattice constants.[4–12] For relaxed GaN and AlN, the piezoelectric polarization is negligible.[13] (However, this component of the polarization depends on the strain of the crystal and may vary with growth method, substrate material, or temperature).

The spontaneous polarization, on the other hand, is large for GaN and AlN; calculations using the Berry-phase approach and local density[14–16] or generalized gradient approximations[15,17] determine the spontaneous polarization is -0.029 C/m^2 and -0.081 C/m^2 for wurtzite GaN and AlN, respectively. This calculation assumes the respective (0001) Ga- and Al-face, suggesting the spontaneous polarization is directed towards the N-face. In addition, the magnitude of the polarization increases with aluminum content, as the spontaneous polarization is sensitive to structural parameters. Therefore, the longer anion-cation bond length along the (0001) axis of AlN corresponds to an increase in magnitude along the c-axis of the wurtzite structure.[18] The polarization of $Al_xGa_{(1-x)}N$ can thus be determined by linear interpolation as displayed in Table I.

This polarization charge gives rise to a bound surface charge,

$$\sigma_{\mathrm{b}} = \bar{P} \cdot \hat{c}. \tag{2}$$

There is thus a negative bound charge of 1.81×10^{13} charges/cm^2 and 5.06×10^{13} charges/cm^2 for the Ga- and Al-face of GaN and AlN crystals, respectively. Consequently, an equivalent positive bound polarization charge exists on the N-face of GaN and AlN. Since the internal electric field of a wide-bandgap semiconductor is zero or near zero, the system adjusts to satisfy surface conditions of near charge neutrality. Therefore, the intrinsic material properties give rise to a distribution of inherent electronic states. The nature and distribution of the compensation charge affect the internal electric field of the materials and ultimately device performance.

This phenomenon is better understood in terms of surface band bending, which is directly related to the space charge region. More specifically, compensation charge in semiconductors, can take two forms: (1) the formation of an internal space-charge layer that consists of ionized donors and defects near the surface, or (2) external charged surface or interface states. These internal and external screening mechanisms are inversely related as shown in Fig. 2, where the larger the compensation from the internal space-charge layer (and thus the smaller the net concentration of surface states), the larger the band bending. The band bending is thus calculated from the density of internal screening charge:

$$\Phi_{\mathrm{s}} = -\frac{qN_{\mathrm{ss}}^2}{2\varepsilon\varepsilon_{\mathrm{o}}N_{\mathrm{d}}}, \tag{3}$$

where q is the charge of an electron, ε is the relative permittivity, ε_{o} is the permittivity of free space, N_{d} is the doping density, and N_{ss} is the net surface charge in charges/cm^2. Assuming a doping density of 10^{17} charges/cm^3 and a net polarization charge of

Table I. Band gap, polarization, and corresponding polarization bound charge for GaN, AlN, and $Al_xGa_{(1-x)}N$

	GaN	AlN	$Al_xGa_{(1-x)}N$
Band gap (eV)	3.4	6.2	3.4 (1 − x) + 6.2x
Spontaneous polarization (C/m^2)	−0.029	−0.081	−0.029 (1 − x) −0.081x
Polarization bound charge (10^{13} charges/cm^2)	1.81	5.06	1.81 (1 − x) + 5.06x

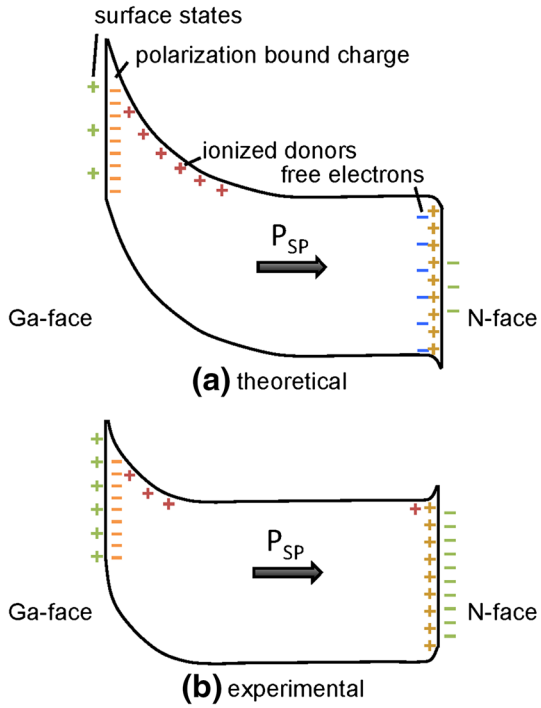

Fig. 2. (Color online) Theoretical (a) and experimental (b) band bending schematic for Ga- and N-face GaN. Both surfaces are screened by ~10^{13} charges/cm^2. (the position of the ionized donors and electrons in the material corresponds to their physical position rather than their energy level within the band gap.) Reprinted from Eller et al.[2] ©2013, American Vacuum Society.

1.81×10^{13} charges/cm^2 for GaN, this calculation suggests a surface potential of −420 V, which corresponds to 420 eV of upwards band bending and an average electric field of 200 MV/m at the surface of GaN. In equilibrium, this large internal field results in inversion or accumulation, and the band bending is thus limited to approximately the band gap of the material, 3.4 eV. (See Fig. 2a.)[19,20] Therefore, ionized donors cannot be solely responsible for the compensation of the polarization bound charge.

Experimental band bending measurements indicate the band bending is well below the band gap. (See Fig. 2b.). In fact, most experimental band bending experiments for n-type Ga-face GaN typically report measurements between 0.3 eV and 1.5 eV.[21–23] These measurements can then determine the concentration of charged surface states from the band bending, where

$$N_{ss} = \sqrt{-\frac{2\Phi_s \varepsilon \varepsilon_o N_d}{q}}. \quad (4)$$

This equation suggests a 0.1 eV change in band bending corresponds to a 3.2×10^{11} charges/cm^2 change in the concentration of surface states.

EXPERIMENT

In this study, we determine the concentration of surface states from the experimentally measured band bending of several different sample surfaces, including the Ga-face of GaN and $Al_{0.25}Ga_{0.75}N$ films as well as the Ga- and N-faces of freestanding GaN. These various sample surfaces enable us to examine different surfaces associated with several polarization bound charge conditions. Freestanding wafers were ~450-μm-thick, n-type, as-grown via hydride vapor phase epitaxy (HVPE) purchased from READE Advanced Materials with a Si doping density of $\sim 8 \times 10^{17}$ cm^{-3}; this doping density determined the position of the Fermi level to be ~0.1 eV lower than the conduction band minimum. Additional n-type Ga-face epitaxial GaN wafers were also used. The samples were 5 ± 1 μm thick, as grown by HVPE on sapphire substrates purchased from READE Advanced Materials. The doping density was still ~10^{17} cm^{-3}, which established a similar Fermi level position. To investigate the effects of a larger concentration of surface bound charge, Ga-face AlGaN was also used with 25% aluminum content as purchased from NTT Advanced Technology. $Al_{0.25}Ga_{0.75}N$ samples were ~50 nm thick, as deposited on Si substrates with a doping density of ~10^{17} cm^{-3}. This doping density ensured a similar Fermi level position as the other samples, ~0.1 eV below the conduction band.

As-received wafers were cleaned *ex situ* via sonication in acetone, methanol, and NH_4OH for 10 min each. Samples were then rinsed in DI water for 1 min and dried with nitrogen. After the chemical cleaning, samples were loaded into an ultra high vacuum system with base pressure of 4×10^{-10} Torr. The inclusive UHV system allowed for *in-situ* cleaning, which reduced the oxygen coverage using NH_3 plasma and additional NH_3 gas annealing at 680°C for 15 min each. The plasma was operated at 100 W with a constant gas flow of 90 sccm and

pressure of 60 mtorr. Characterization was subsequently conducted using *in-situ* XPS.

More specifically, XPS spectra were used to determine the stoichiometric ratios and surface band bending. These spectra were obtained at a base pressure of 8×10^{-10} Torr. Mg Kα (=1253.6 eV) x-ray radiation was used as a radiation source, except when scanning the C 1s peak; the Ga LMM Auger lines and C 1s peak overlap, and, therefore, Al Kα (=1486.6 eV) x-rays were used. The non-monochromatic x-ray source used a 4.4 A filament current, 16 mA emission current, and 13 kV accelerating voltage. Survey scans were repeated 30–80 times with a pass energy of 20 eV. The spectra were dispersed with a Fisons Clam II hemispherical analyzer at a resolution of ~1.0 eV. Through curve fitting of the core level peaks, the peak positions could be resolved to ±0.1 eV. These measurements included adjustments according to a calibration using a gold foil; typical corrections were −0.1 and −0.2 eV for respective Mg and Al radiation sources. XPS measurements were also used to determine the concentration and the atomic ratio of constituents near the surface; C 1s and O 1s spectra indicated the effectiveness of the cleaning process, while Ga 3d and N 1s spectra indicated the stoichiometric ratio of the GaN at the surface.

RESULTS

The oxygen coverage was defined as the number of absorbed oxygen atoms per Ga (Al) or N atoms at the c plane surface, where one oxygen atom per surface lattice site referred to a single monolayer (ML) of coverage. This ratio was calculated by the following[24]:

$$\Theta_o = \frac{I_O}{S_O}\left(\frac{S_{Ga}}{I_{Ga}}\right)\sum_{n=0}^{\infty}\exp\left[\frac{-nd_{GaN}}{\lambda_{Ga}Cos[\phi]}\right], \qquad (5a)$$

where I_{Ga} and I_O were the integrated intensities of the respective Ga 3d and O 1s peaks, S_O and S_{Ga} were the atomic sensitivity factors for respective O 1s and Ga 3d (0.66 and 0.31),[19] λ_{Ga} was the inelastic mean free path of Ga 3d electrons with kinetic energies ~1200 eV (~24 Å),[25] ϕ was the angle between the normal direction and the analyzer (20°), and d was the distance between two Ga planes (2.6 Å). For $Al_{0.25}Ga_{0.25}N$, this calculation was modified, where one in every four Ga atoms was replaced with an Al atom, giving

$$\Theta_o = \frac{I_O}{S_O}\Bigg/\left[\frac{I_{Ga}}{S_{Ga}\sum_{n=0}^{\infty}\exp\left[\frac{-nd_{GAlaN}}{\lambda_{Ga}Cos[\phi]}\right]} + \frac{I_{Al}}{S_{Al}\sum_{n=0}^{\infty}\exp\left[\frac{-nd_{GAlaN}}{\lambda_{Al}Cos[\phi]}\right]}\right], \qquad (5b)$$

where I_{Al} was the integrated intensity for the Al 2p peak, S_{Al} was the atomic sensitivity factor for Al 2p (0.185), λ_{Al} was the approximate average inelastic mean free path of Al 2p electrons with kinetic energies ~1400 eV (~24 Å),[26] and d_{AlGaN} was the distance between two Ga/Al planes (2.6 Å). The oxygen coverage on each sample after the different cleaning states is summarized in Table II, and the XPS core levels are shown in Fig. 3. In general, the AlGaN surfaces are more resistant to oxygen reduction;[27–29] this is expected given the difficulty of breaking Al–O bonds during the cleaning process. Moreover, the NH_3 cleaning reduced carbon below the XPS detection limit.

The atomic concentration ratios of the samples were also determined after the different processing steps from relative XPS intensities, as shown in Fig. 4 and summarized in Table III.

Band bending (BB) of oxygen-terminated GaN and AlGaN was also calculated from the position of the Ga 3d core level and inherent material properties, as shown in Fig. 5:

$$BB = (E_V - E_{CL})_{GaN} + E_g - E_{CL,XPS} + E_C, \qquad (6)$$

where E_C was the position of the conduction band with respect to the Fermi level as determined by the doping density (−0.1 eV), E_g was the band gap of the material ($E_{g,GaN}$ = 3.4 eV and $E_{g,AlGaN}$ = 4.0 eV[30]), and $E_{Cl,\ XPS}$ was the position of the Ga 3d core level for GaN and Al 2p core level for AlGaN. It is worth noting here that this analysis focused on the Ga 3d peak, where the core level intensity and position were less sensitive to the overlayer, thereby providing more reliable band bending measurements. Additionally, $(E_{CL} - E_V)_{GaN}$ represented the binding energy difference of the core level of Ga 3d in GaN with respect to the VBM. According to electronic state studies of GaN,[31–33] the difference between the Ga 3d core level and the valence band maximum was 17.7 eV–17.8 eV. In

Table II. Oxygen coverage (in ML) on N-face GaN, Ga-face GaN, and Ga-face AlGaN as determined after the various cleaning steps as given by XPS

Oxygen coverage	N-face GaN	Ga-face GaN	Ga-face $Al_{0.25}Ga_{0.75}N$
As received	4.5	5.1	2.6
Ex situ cleaning	2.6	3.1	2.2
In situ cleaning	1.1	1.1	1.8

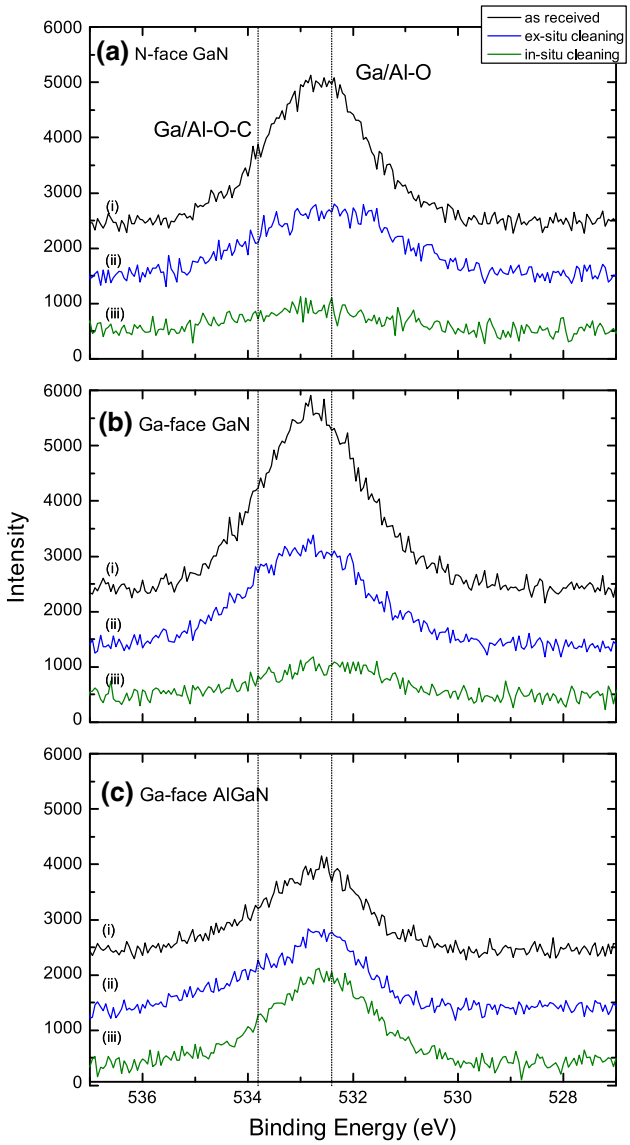

Fig. 3. (Color online) O 1s peak for N-face GaN (a), Ga-face GaN (b), and Ga-face $Al_{0.25}Ga_{0.75}N$ (c) as received (*i*), after *ex-situ* cleaning (*ii*), and after *in-situ* cleaning (*iii*). Note that core levels were shifted to the corresponding flat band position, allowing direct comparison of the oxygen states.

this study, 17.8 eV was assumed for $(E_{CL} - E_V)_{GaN}$. Similar electronic-state studies of $Al_{0.25}Ga_{0.75}N$ indicated 17.5 eV[34] and 71.5 eV[35] were the respective differences between the Ga 3d and Al 2p core levels and the valence band maximum, which were used to determine the band bending at the AlGaN surface. Please note that, while the Ga and Al core level peaks include a component due to Ga–O and Al–O bonding, this component does not affect the peak position. The experimental band bending of each sample after various stages of cleaning is summarized in Table IV, and the corresponding external compensation charge is summarized in Table V.

These results demonstrated there was a relationship between film content and band bending. In particular, it was revealed that band bending was inversely related to oxygen coverage as shown in Fig. 6a and positively correlated to nitrogen content as shown in Fig. 6b. In addition, while there was a small disparity in the band bending on the N- and Ga-face—which may be the result of different interface dipoles[36]—all three surfaces were characterized by similar band bending after cleaning, ranging from −0.1 eV to 0.9 eV. The magnitude of this band bending suggests the presence of an electronic surface state responsible for Fermi level pinning ~0.1 eV to 0.9 eV below the conduction band edge. Moreover, the similarity of the band bending regardless of the polarization bound charge suggests this pinning state can accommodate charge transfer to compensate both positive and negative charge. This pinning state is thus as modeled in Fig. 7.

DISCUSSION

In order to identify the microscopic nature of this pinning state, we have considered surface reconstructions, defect states, and adsorbates; however, direct comparison between experiment and theory is often not a straightforward means of identifying the microscopic nature of a surface.

To date, most related theoretical research has focused on the nature of pinning states on Ga-face GaN as dependent on surface reconstructions. For example, at the Ga-face surface, several (2×2) surface reconstructions are thought to be the most stable, including the gallium adatom, nitrogen adatom, and gallium vacancy structures.[37,38] Nevertheless, most experimental studies do not explicitly agree with these results, where (1×1), (2×2), (2×4), (5×5), and (6×4) reconstructions have all been observed.[39–41] In other words, although the existence of Fermi level pinning surface states has been well documented in GaN-based materials,[42–44] a microscopic understanding of these states and their dependence on polarity is still unclear. The discrepancy between experimental and theoretical values is likely the result of two factors. First, a detailed understanding of the theoretical and experimental band structure and related density of states of experimentally relevant GaN surface reconstructions is lacking. Second, theoretical studies generally assume clean, ordered surface conditions when such surfaces rarely exist; actual GaN surfaces are commonly oxidized or metal rich. Recent studies have attempted to rectify this disparity, where Himmerlich et al.[45] described experimental and theoretical surface studies to determine the microscopic surface conditions.

However, these perfectly ordered surface reconstructions are not sufficient to explain observed Fermi level pinning; it is thus more likely these results were caused by a defect state. Given the magnitude of the experimentally observed band bending and the proportional relationship between the band bending and nitrogen concentrations, it

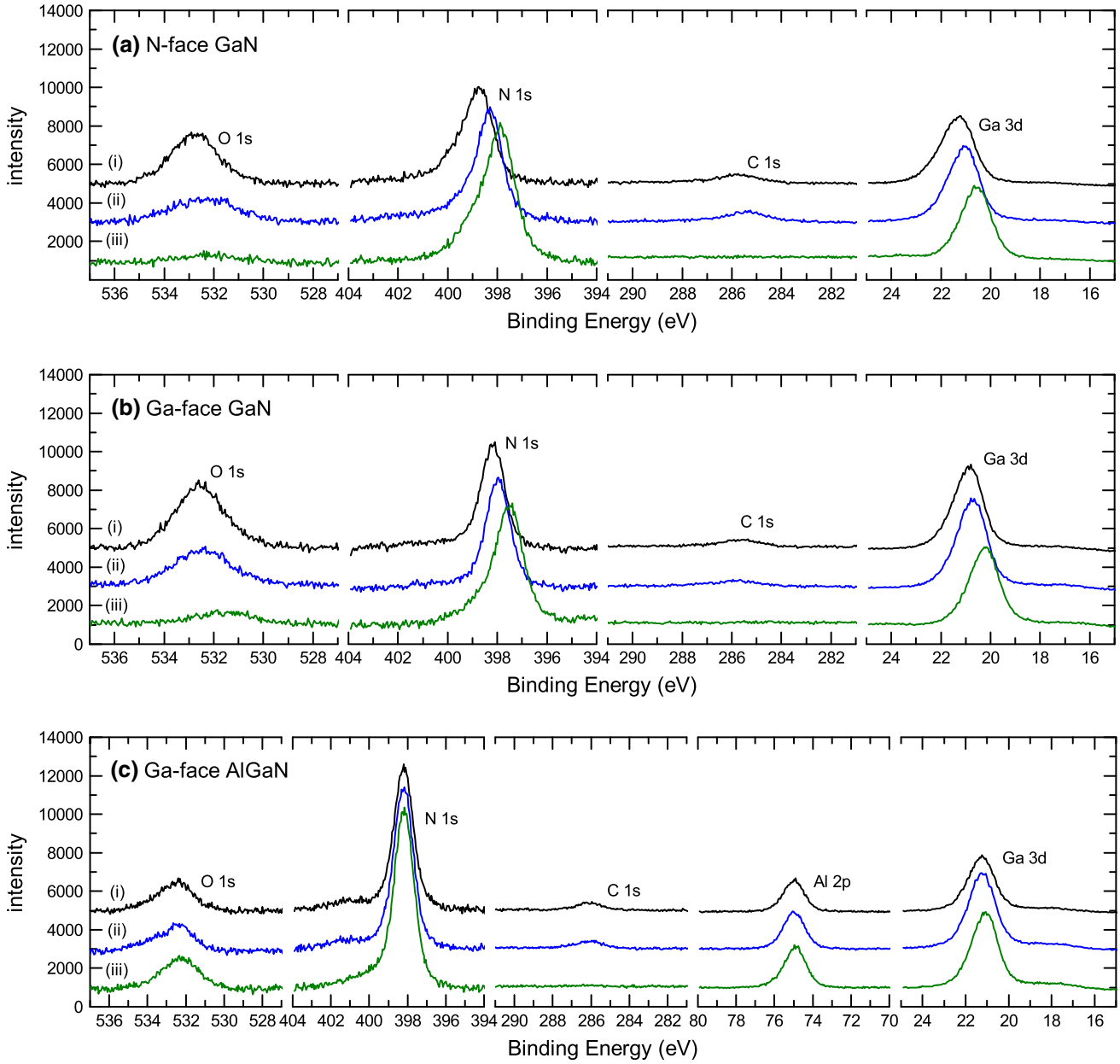

Fig. 4. (Color online) XPS results for N-face GaN (a), Ga-face GaN (b), and Ga-face $Al_{0.25}Ga_{0.75}N$ (c) as received (*i*), after *ex situ* cleaning (*ii*), and after *in-situ* cleaning (*iii*).

Table III. Atomic ratio of N/Ga(Al) as determined from Al 2p, Ga 3d, and N 1s core level intensities, respective atomic sensitivity factors of 0.19, 0.31, and 0.42, and effective attenuation lengths as determined from the NIST database[58]

Atomic ratios	N-face GaN	Ga-face GaN	Ga-face $Al_{0.25}Ga_{0.75}N$
As received	0.92	0.74	1.17
Ex situ cleaning	1.02	0.78	0.84
In situ cleaning	2.03	1.42	1.28

has been proposed that the observed pinning state behavior is related to a nitrogen vacancy or gallium dangling bond. These states have been theoretically and experimentally determined to be located ~0.37 eV[46] or 0.5 eV–0.7 eV[47] below the conduction band edge, which agrees with the experimental

findings in this research as well. Furthermore, these defect states have been linked back to device behavior, where Hashizume and Hasegawa[46] demonstrated that passivating GaN-based samples with nitrogen improves device reliability.

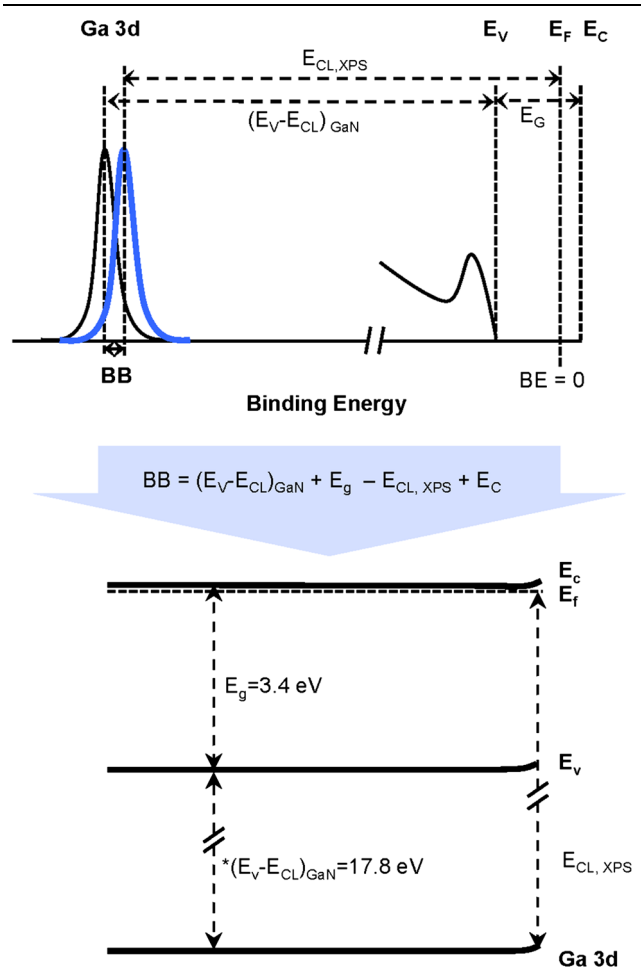

Fig. 5. (Color online) Surface bend bending measurements (bottom) were determined from the position the Ga 3d core level as determined from XPS (top) by the given equation (middle).

While this evidence is suggestive, there are several other factors that may affect the band bending on these samples as well. In particular, we cannot overlook the effects of oxygen coverage. To date, a number of studies have investigated the effects of various *ex-situ* and *in-situ* treatments, including HF, NH_4OH, annealing, as well as N_2 and H_2 plasma.[2,48–54] These studies demonstrate the difficulty in removing native oxygen, likely GaO_2 or Ga_2O_3,[51] from GaN surfaces without damaging the surface reconstruction, as it leaves nitrogen vacancies and/or gallium dangling bonds. Consequently, the cleaning method used should passivate these states. This was the case in this experiment and may explain the reciprocal nature between the oxygen coverage and nitrogen content as shown in Fig. 6. On the other hand, it may be possible that the oxygen coverage introduces additional charge states. For example, there is evidence that dissociation of H_2O and O_2 on GaN surfaces introduces O and OH^- groups on the surface.[53,54] Removal of this negative charge would thus describe the increase in band bending on the Ga-face as well. It is thus unclear whether the oxygen coverage contributes to the band bending as well, especially on the N face. Moreover, the plasma used in the cleaning may also influence the band bending. While NH_3 plasma annealing has been shown to reduce oxygen effectively, the plasma may also introduce interstitial nitrogen. Therefore, an additional component of the band bending may not necessarily be attributable to surface reconstructions or point defects.

In reality, these explanations are not mutually exclusive. It is likely that nitrogen interstitials, oxygen adsorbates, and vacancies influence the observed band bending at different cleaning stages. Furthermore, additional research has provided evidence for a fixed charge at the interface,[55–57] which may affect the Fermi level pinning position;

Table IV. Band bending (in eV) for N-face GaN, Ga-face GaN, and Ga-face AlGaN as determined after the various cleaning steps as given by XPS

Band bending	N-face GaN	Ga-face GaN	Ga-face $Al_{0.25}Ga_{0.75}N$
As received	−0.1	0.2	0.2
Ex situ cleaning	0.1	0.4	0.2
In situ cleaning	0.6	0.9	0.4

Table V. Concentration of external compensation charge (10^{13} charges/cm^2) on N-face GaN, Ga-face GaN, and Ga-face AlGaN as determined after the various cleaning steps as given by XPS

Net external compensation	N-face GaN	Ga-face GaN	Ga-face $Al_{0.25}Ga_{0.75}N$
As received	−1.8	+1.8	+2.6
Ex situ cleaning	−1.8	+1.7	+2.6
In situ cleaning	−2.0	+1.5	+2.5

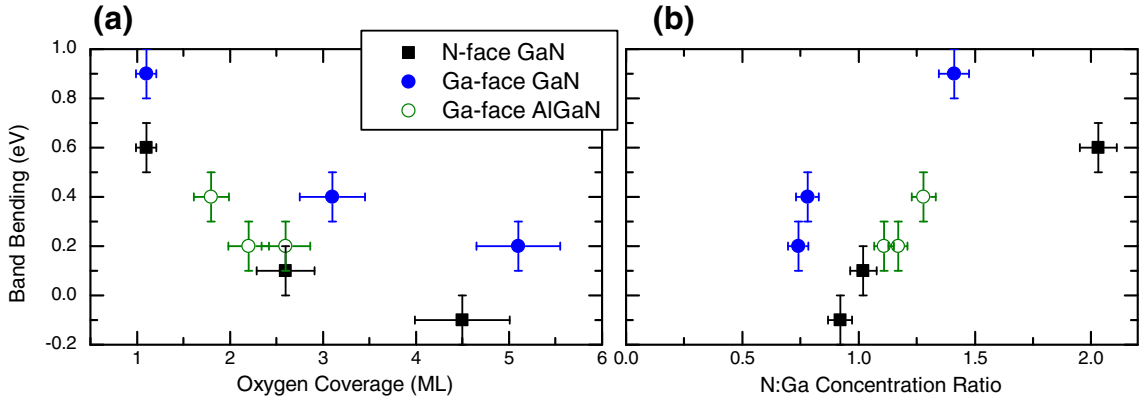

Fig. 6. (Color online) Correlation between the surface band bending and film content, i.e. oxygen coverage (a) and relative nitrogen surface concentration (b) for N-face GaN, Ga-face GaN, and Ga-face $Al_{0.25}Ga_{0.75}N$.

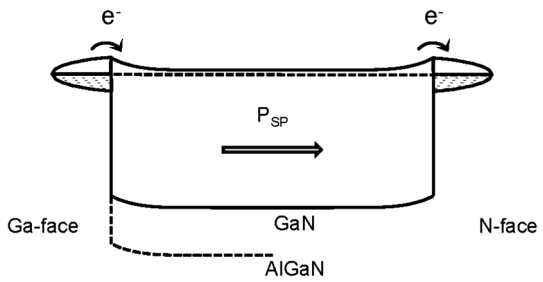

Fig. 7. Suggested charge transfer model for pinning state on N- and Ga-face GaN and AlGaN.

however, without additional CV measurements, it is difficult to resolve the discrepancy between the electrical measurements and photoemission measurements.

CONCLUSION

In summary, we have used XPS to determine the net concentration of surface states on N-face GaN, Ga-face GaN, and Ga-face $Al_{0.25}Ga_{0.75}N$. The results demonstrated a similar band bending regardless of the magnitude or direction of the polarization bound charge. (There is a disparity between the N- and Ga-face; however, this difference is likely the result of an interface dipole, which will be explored further.) Specifically, the band bending varies from −0.1 eV to 0.9 eV on these samples, which indicated that there was likely a Fermi pinning state ~0.4 eV to 0.8 eV below the conduction band minimum. We suggested the observed pinning state was related to the nitrogen-related defect or gallium dangling bond, as supported by experimental and literary results—though the state was not directly observed. This proposal is consistent with other experimental and theoretical research; however, there were likely additional mechanisms that influence surface states. In particular, it is still unclear how oxygen adsorbates impact the electronic states configuration. Moreover, the plasma cleaning process likely introduced additional nitrogen interstitial or surface states and affected the band bending. Future research will continue to investigate the effects of polarity with more emphasis on surface bonding to better understand the microscopic nature of these states and their effects on the band bending at the surface of GaN-based materials as well as correlate CV and photoemission measurements to resolve potential inconsistencies.

ACKNOWLEDGEMENT

This research was supported by the Office of Naval Research through the DEFINE MURI program, N00014-10-1-0937.

REFERENCES

1. U.K. Mishra, P. Parikh, and Y.F. Wu, *Proc. IEEE* 90, 1022 (2002).
2. B.S. Eller, J. Yang, and R.J. Nemanich, *J. Vac. Sci. Technol. A* 31, 050807 (2013).
3. Y. Niiyama, S. Ootomo, J. Li, T. Nomura, S. Kato, and T.P. Chow, *Semicond. Sci. Technol.* 25, 125006 (2010).
4. V.A. Savastenko and A.U. Sheleg, *Phys. Status Solidi A* 48, K135 (1978).
5. Y. Takagi, M. Ahart, T. Azuhata, T. Sota, K. Suzuki, and S. Nakamura, *Physica B* 219–220, 547 (1996).
6. A. Polian, M. Grimsditch, and I. Grezegory, *J. Appl. Phys.* 79, 3343 (1996).
7. R.B. Schwartz, K. Khachaturyan, and E.R. Webber, *Appl. Phys. Lett.* 70, 1122 (1997).
8. C. Deger, E. Born, H. Angerer, O. Ambacher, M. Stutzmann, J. Hornsteiner, E. Riha, and G. Fischerauer, *Appl. Phys. Lett.* 72, 2400 (1998).
9. K. Tsubouchi and N. Mikoshiba, *IEEE Trans. Sonics Ultrason.* 32, 634 (1985).
10. L.E. McNeil, M. Grimsditch, and R.H. French, *J. Am. Ceram. Soc.* 76, 1132 (1993).
11. K. Kim, W.R.L. Lambrecht, and B. Segall, *Phys. Rev. B* 53, 16310 (1996).
12. A.F. Wright, *J. Appl. Phys.* 82, 2833 (1997).
13. O. Ambacher, J. Smart, J.R. Shealy, N.G. Weimann, K. Chu, M. Murphy, W.J. Schaff, L.F. Eastman, R. Dimitrov, L. Wittmer, M. Stutzmann, W. Rieger, and J. Hilsenbeck, *J. Appl. Phys.* 85, 3222 (1999).
14. F. Bernardini, V. Fiorentini, and D. Vanderbilt, *Phys. Rev. B* 56, R10024 (1997).
15. F. Bernardini, V. Fiorentini, and D. Vanderbilt, *Phys. Rev. B* 63, 193201 (2001).
16. Y. Duan, J. Li, S.-S. Li, and J.-B. Xia, *J. Appl. Phys.* 103, 023705 (2008).

17. K. Shimada, A. Zenpuku, K. Fukiwara, K. Hazu, S.F. Chichibu, M. Hata, H. Sazawa, T. Takada, and T. Sota, *J. Appl. Phys.* 110, 074114 (2011).
18. E.T. Yu, X.Z. Dang, P.M. Asbeck, S.S. Lau, and G.J. Sullivan, *J. Vac. Sci. Technol. B* 17, 1742 (1999).
19. J. Yang, B.S. Eller, C. Zhu, C. England, and R.J. Nemanich, *J. Appl. Phys.* 112, 053710 (2012).
20. H.W. Jang, J.-H. Lee, and J.-L. Lee, *Appl. Phys. Lett.* 80, 3955 (2002).
21. M. Hong, K.A. Anselm, J. Kwo, H.M. Ng, J.N. Baillargeon, A.R. Kortan, J.P. Mannaerts, A.Y. Cho, C.M. Lee, J.I. Chyi, and T.S. Lay, *J. Vac. Sci. Technol. B* 18, 1453 (2000).
22. Y.Q. Wu, T. Shen, P.D. Ye, and G.D. Wilk, *Appl. Phys. Lett.* 90, 143504 (2007).
23. W.J. Mecouch, B.P. Wagner, Z.J. Reitmeier, R.F. Davis, C. Pandarinath, B.J. Rodriguez, and R.J. Nemanich, *J. Vac. Sci. Technol. A* 23, 72 (2005).
24. V.M. Bermudez, *J. Appl. Phys.* 80, 1190 (1996).
25. M. Krawczyk, L. Zommer, A. Jablonski, I. Grzegory, and M. Bockowski, *Surf. Sci.* 566–568, 1234 (2004).
26. H.-H. Wu, Ph.D. Thesis. Ohio State University, 2011.
27. B. Brennan, X. Qin, H. Dong, J. Kim, and R.M. Wallace, *Appl. Phys. Lett.* 101, 211604 (2012).
28. X. Qin, H. Dong, B. Brennan, A. Azacatl, J. Kim, and R.M. Wallace, *Appl. Phys. Lett.* 103, 221604 (2013).
29. X. Qin, B. Brennan, H. Dong, J. Kim, C.L. Hinkle, and R.M. Wallace, *J. Appl. Phys.* 113, 244102 (2013).
30. R.R. Pela, C. Caetano, M. Marques, L.G. Ferreira, J. Furthmuller, and L.K. Teles, *Appl. Phys. Lett.* 98, 151907 (2011).
31. T.E. Cook Jr, C.C. Fulton, W.J. Mecouch, R.F. Davis, G. Lucovsky, and R.J. Nemanich, *J. Appl. Phys.* 94, 7155 (2003).
32. J.R. Waldrop and R.W. Grant, *Appl. Phys. Lett.* 68, 2879 (1996).
33. J. Hedman and N. Mårtensson, *Phys. Scr.* 22, 176 (1980).
34. Y.L. Chiou and C.T. Lee, *IEEE Trans. Electron Devices* 58, 3869 (2011).
35. M.H.S. Owen, M.A. Bhuiyan, Q. Zhou, Z. Zhang, J.S. Pan, and Y.-C. Yeo, *Appl. Phys. Lett.* 104, 091605 (2014).
36. J. Yang, B.S. Eller, and R.J. Nemanich, *J. Appl. Phys*. (submitted).
37. J.E. Northrup, J. Neugebauer, R.M. Feenstra, and A.R. Smith, *Phys. Rev. B* 61, 9932 (2000).
38. D. Segev and C.G. Van de Walle, *Surf. Sci.* 601, L15 (2007).
39. A.R. Smith, R.M. Feenstra, D.W. Greve, M.-S. Shin, M. Skowronski, J. Neugebauer, and J.E. Northrup, *Surf. Sci.* 423, 70 (1999).
40. S.W. King, C. Ronning, R.F. Davis, M.C. Benjamin, and R.J. Nemanich, *J. Appl. Phys.* 84, 2086 (1998).
41. S. Vézian, F. Semond, J. Massies, D.W. Bullock, Z. Ding, and P.M. Thibado, *Surf. Sci.* 541, 242 (2003).
42. A.R. Smith, R.M. Feenstra, D.W. Greve, M.S. Shin, M. Skowronski, J. Neugebauer, and J.E. Northrup, *J. Vac. Sci. Technol. B* 16, 2242 (1998).
43. C.G. Van de Walle and D. Segev, *J. Appl. Phys.* 101, 081704 (2007).
44. L. Ivanova, S. Borisova, H. Eisele, M. Dahne, A. Laubsch, and Ph Eben, *Appl. Phys. Lett.* 93, 192110 (2008).
45. M. Himmerlich, L. Lymperakis, R. Gutt, P. Lorenz, J. Neugebauer, and S. Krischok, *Phys. Rev. B* 88, 125304 (2013).
46. T. Hashizume and H. Hasegawa, *Appl. Surf. Sci.* 234, 387 (2004).
47. D. Segev and C.G. Van de Walle, *Europhys. Lett.* 76, 305 (2006).
48. S.W. King, J.P. Barnak, M.D. Bremser, K.M. Tracy, C. Ronning, R.F. Davis, and R.J. Nemanich, *J. Appl. Phys.* 84, 5248 (1998).
49. T. Hashizume, S. Ootomo, T. Inagaki, and H. Hasegawa, *J. Vac. Sci. Technol. B* 21, 1828 (2003).
50. R.D. Long and P.C. McIntyre, *Mater* 5, 1297 (2012).
51. C.L. Hu, J.Q. Li, Y.F. Zhang, X.L. Hu, N.X. Lu, and Y. Chen, *Chem. Phys. Lett.* 424, 273 (2006).
52. R. Meunier, A. Torres, and M. Charles, *ECS Trans.* 50, 451 (2013).
53. J. Elsner, R. Gutierrez, B. Hourahine, R. Jones, M. Haugk, and Th Frauenheim, *Solid State Comm.* 108, 953 (1998).
54. V.M. Bermudez and J.P. Long, *Surf. Sci.* 450, 98 (2000).
55. M. Esposto, S. Krishnamoorthy, D.N. Nath, S. Bajaj, T.-H. Hung, and S. Rajan, *Appl. Phys. Lett.* 99, 1233503 (2011).
56. S. Ganguly, J. Verma, G. Li, T. Zimmermann, H. Xing, and D. Jena, *Appl. Phys. Lett.* 99, 193504 (2011).
57. J. Son, V. Chobpattana, B.M. McSkimming, and S. Stemmer, *Appl. Phys. Lett.* 101, 102905 (2012).
58. NIST, *Electron Effective-Attenuation-Length Database, SRD-82, Version 1.1* (Gaitherburg: National Institute of Standards and Technology, 2003).